

1 Impact Statement

2  
3 The causal mechanisms of global glaciations are poorly understood. The transition to a  
4 Neoproterozoic Snowball Earth after more than 1 Gyr without glaciation represents the  
5 most dramatic episode of climate change in the geological record. Here we present new  
6 Re-Os geochronology, which, together with existing U-Pb ages, reveal that the glacial  
7 period in NW Canada lasted ~55 Myr. Additionally, we present a novel method to track  
8 tectonic influences on these climatic perturbations with the first high- resolution coupled  
9 Os-Sr isotope curve across the transition from an ice-free world to a Neoproterozoic  
10 Snowball Earth. The data indicates that increases in mantle-derived, juvenile material  
11 emplaced onto continents and subsequently weathered into the oceans led to enhanced  
12 consumption and sequestration of CO<sub>2</sub> into sediments.

13

14 *Classification:* PHYSICAL SCIENCES

15 *Title:* Weathering the Snowball

16 *Authors:* Alan D. Rooney<sup>1</sup>, Francis A. Macdonald<sup>1</sup>, Justin V. Strauss<sup>1</sup>, Francis Ö. Dudás<sup>2</sup>,  
17 Christian Hallmann<sup>2,3,4</sup>, David Selby<sup>5</sup>

18 *Affiliations:* <sup>1</sup> Department of Earth and Planetary Sciences, Harvard University, Cambridge,  
19 MA 02138; <sup>2</sup> Department of Earth, Atmospheric and Planetary Sciences, Massachusetts  
20 Institute of Technology, Cambridge, MA 02139; <sup>3</sup> Max-Planck-Institute for  
21 Biogeochemistry, Hans-Knöll-Strasse 10, 07745 Jena, Germany; <sup>4</sup> MARUM, University of  
22 Bremen, Leobener Strasse, 28359 Bremen, Germany; <sup>5</sup> Department of Earth Sciences,  
23 Durham University, Durham, DH1 3LE, UK.

24 *Corresponding Author:* Alan D. Rooney, Department of Earth and Planetary Sciences,  
25 Harvard University, Cambridge, MA 02138, Tel: 617-496-2412, Email:  
26 alanrooney@fas.harvard.edu

27 *Keywords:* Sturtian, Neoproterozoic, Cryogenian, Snowball Earth, Re-Os geochronology,  
28 Strontium isotopes

29

30 **Abstract.**

31 After nearly a billion years with no evidence for glaciation, ice advanced to equatorial  
32 latitudes at least twice between 717 and 635 Ma. Although the initiation mechanism of  
33 these Neoproterozoic Snowball Earth events has remained a mystery, the broad  
34 synchronicity of rifting of the supercontinent Rodinia, the emplacement of large igneous  
35 provinces at low latitude, and the onset of the Sturtian glaciation has suggested a tectonic  
36 forcing. We present new Re-Os geochronology and high-resolution Os and Sr isotope  
37 profiles bracketing Sturtian-age glacial deposits of the Rapitan Group in NW Canada.  
38 Coupled with existing U-Pb dates, the post-glacial Re-Os date of  $662.4 \pm 3.9$  Ma  
39 represents the first direct geochronological constraints on both the onset and demise of a  
40 Cryogenian glaciation from the same continental margin, and suggest a 55 Myr duration of  
41 the Sturtian glacial epoch. The Os and Sr isotope data allow us to assess the relative  
42 weathering input of old radiogenic crust and more juvenile, mantle-derived substrate. The  
43 pre-glacial isotopic signals are consistent with an enhanced contribution of juvenile  
44 material to the oceans and glacial initiation through enhanced global weatherability. In  
45 contrast, post-glacial strata feature radiogenic Os and Sr isotope compositions indicative of  
46 extensive glacial scouring of the continents and intense silicate weathering in a post-  
47 Snowball Earth hothouse.

48

49 /body/

50 The Snowball Earth hypothesis predicts that Neoproterozoic glaciations were global and  
51 synchronous at low-latitudes and that deglaciation occurred as a result of the build-up of  
52  $p\text{CO}_2$  to extreme levels resulting in a “greenhouse” aftermath (1, 2). The temporal  
53 framework of Cryogenian glaciations is built on chemostratigraphy and correlation of  
54 lithologically distinct units, such as glaciogenic deposits, iron formation, and cap  
55 carbonates (3), tied to the few successions that contain volcanic rocks dated using U-Pb  
56 zircon geochronology (4). In strata lacking horizons suitable for U-Pb geochronology, Re-  
57 Os geochronology can provide depositional ages on organic-rich sedimentary rocks  
58 bracketing glaciogenic strata (5, 6). Moreover, Os isotope stratigraphy can be used as a  
59 proxy to test for super-greenhouse weathering during deglaciation (7). In a Snowball Earth  
60 scenario we can make specific predictions for Cryogenian weathering:  $\text{CO}_2$  consumption  
61 via silicate weathering should increase before glaciation, stagnate during the glaciation, and  
62 increase again during deglaciation. However, the use of a single weathering proxy to  
63 provide evidence for such a scenario, such as Sr isotopes from marine carbonates, is limited  
64 both by lithological constraints and an inability to distinguish between the amount of  
65 weathering and the composition of what is being weathered (8). The short residence time of  
66 Os in the present-day oceans (<10 kyr) (9) provides a complementary higher resolution  
67 archive to Sr isotopes and thus, new insights into the nature of extreme fluctuations in the  
68 Earth’s climate as documented herein.

69

70 **Stratigraphy of the Neoproterozoic Windermere Supergroup**

71 The Neoproterozoic Windermere Supergroup is spectacularly exposed in the Mackenzie  
72 Mountains of NW Canada and comprises an ~7 km thick mixed carbonate and siliciclastic  
73 marine succession (Fig. 1, Fig. S1). The Coates Lake Group of the Mackenzie Mountains  
74 forms the base of the Windermere Supergroup and consists of siliciclastic, carbonate and  
75 evaporitic strata of the Thundercloud, Redstone River and Coppercap formations. The  
76 Coates Lake Group unconformably overlies the Little Dal Basalt, which has been correlated  
77 geochemically with the Tsezotene sills (10), a 777 ± 2.5/-1.8 Ma ( $^{206}\text{Pb}/^{238}\text{U}$  multi-grain  
78 zircon thermal ionization mass spectrometry date) quartz diorite plug near Coates Lake  
79 (11), and the ~780 Ma Gunbarrel magmatic event (12).

80         Near Coates Lake, the Coppercap Formation, is ~410 m thick and is separated into 6  
81 units (CP1-CP6 in Fig. 2). The Coppercap Formation culminates with a partially  
82 dolomitized unit of carbonate conglomerate, with minor sandstone, chert and evaporite  
83 (CP6), and is overlain by siltstone and diamictite of the Rapitan Group (Fig. 2).

84         Economic copper deposits grading 3.9% occur in unit CP1 of the Coppercap  
85 Formation in a 1 m-thick interval (13, 14). These formed directly below the flooding  
86 surface at the base of CP2 (14). Above this, in units CP2-CP5, there is no evidence for  
87 mineralization, exposure, or significant sulfate reduction, although minor evaporite and  
88 metal showings are present in association with the exposure surfaces at the top of unit CP6.

89         Regionally, the Rapitan Group rests unconformably on the Coates Lake Group, but  
90 locally the contact can be gradational (15). In the Ogilvie Mountains, the age of the Rapitan  
91 Group is constrained by a  $^{206}\text{Pb}/^{238}\text{U}$  single grain chemical abrasion-isotope dilution-  
92 thermal ionization mass spectrometry (CA-ID-TIMS) zircon date of  $717.4 \pm 0.1$  Ma on a  
93 rhyolite from the underlying Mount Harper Volcanic Complex, and  $716.5 \pm 0.2$  Ma on a

94 volcanic tuff within the overlying glaciogenic diamictites indicating that glaciation  
95 commenced ~717 Ma (4). The Rapitan Group is composed of three formations consisting of  
96 stratified and massive glaciogenic diamictites with minor iron formation (16, 17). The  
97 lowest unit, the Mount Berg Formation, is present only in the southern Mackenzie  
98 Mountains. The overlying Sayunei Formation is locally more than 600 m thick and  
99 comprises ferruginous, maroon to dark brown turbiditic siltstone, sandstone, debrites and  
100 intervals of stratified and massive glacial diamictite with dropstones of carbonate, basalt  
101 and rare granitoid clasts (16, 17). Discontinuous lenticular bodies of hematite-jaspillite iron  
102 formation are present near the top of the Sayunei Formation when they are not eroded by  
103 the overlying Shezal Formation (17, 18). The uppermost unit of the Rapitan Group, the  
104 Shezal Formation, consists of >600 m of green-grey, yellow weathering stratified and  
105 massive glacial diamictite interbedded with decameter-scale units of mudstone, siltstone  
106 and sandstone, which in some localities unconformably overlies the Sayunei Formation (11,  
107 15, 19). Clast composition in the Shezal Formation is highly variable with an abundance of  
108 carbonate, altered basic volcanic, sandstone, chert and less common metamorphic pebbles  
109 and cobbles (16, 17). An extended duration for deposition of the Rapitan Group is  
110 supported by internal unconformities and paleomagnetic poles that shift ~40° from the  
111 Mount Berg to Sayunei formations (20).

112         Locally, the basal Twitya Formation of the Hay Creek Group conformably overlies  
113 the Rapitan Group, but regionally various parts of the Twitya Formation rest  
114 unconformably on underlying strata (19). Where conformable, such as at Mountain River,  
115 the basal Twitya Formation consists of a 0-40 m thick ‘cap carbonate’ that is characterized  
116 by finely-laminated lime mudstone and siltstone with minor graded beds and sedimentary

117 slump folds (Fig. 2). The lower Twitya Formation is part of a transgressive sequence that  
118 passes upwards into fetid, pyritic black shale and then into hundreds of meters of grey-  
119 green siltstone and sandstone turbidites. These strata are succeeded by variable siliciclastic  
120 and carbonate strata of the Keele Formation and glaciogenic deposits of the Stelfox  
121 Member. The Stelfox Member of the Ice Brook Formation consists of massive diamictite  
122 with striated clasts (21) and is capped by the Ravenstroat Formation, a white to buff-  
123 colored dolostone (17, 22), which hosts sedimentological and geochemical features  
124 characteristic of globally distributed ~635 Ma Marinoan cap carbonates (2, 23).

125

## 126 **Re-Os Geochronology**

127 Organic-lean (<0.5% TOC) cryptalgal laminites of the Coppercap Formation were obtained  
128 from drill core and outcrop near Coates Lake (Figs. 1, 2). Core samples were analysed for  
129 major and minor elements, carbonate content, C, Sr, and Os isotope chemostratigraphy, and  
130 four samples were used for Re-Os geochronology and Os isotope stratigraphy (see SI for  
131 details).

132 A Re-Os age of  $732.2 \pm 3.9$  Ma (4.7 Ma including  $^{187}\text{Re}$  decay constant uncertainty,  
133  $n = 4$ , Mean Square of Weighted Deviates [MSWD] = 1.9,  $2\sigma$ , initial  $^{187}\text{Os}/^{188}\text{Os} = 0.15 \pm$   
134 0.002) was obtained from the Coppercap Formation (Fig. 3a). In conjunction with existing  
135 U-Pb zircon ages from the Ogilvie Mountains, this Re-Os age indicates an interval ~15 Myr  
136 between deposition of unit CP4 of the Coppercap Formation and Rapitan Group  
137 glaciogenic strata (Figs. 1, 2).

138 Organic-rich (>0.5% TOC) micritic limestone of the post-glacial basal Twitya  
139 Formation was sampled from outcrop near Mountain River (64°32'04"N, 129°23'42"W).

140 The ‘cap’ limestone was sampled at ~0.5 m resolution for Sr, Os and C isotope  
141 chemostratigraphy (24), and a thin (<20 cm) horizon less than 2 m above the Rapitan-  
142 Twitya contact was sampled for Re-Os geochronology (Fig. 2). The basal Twitya  
143 Formation yielded a Re-Os age of  $662.4 \pm 3.9$  Ma (4.6 Ma including  $^{187}\text{Re}$  decay constant  
144 uncertainty,  $n = 7$ , MSWD = 1.9,  $2\sigma$ , initial  $^{187}\text{Os}/^{188}\text{Os} = 0.54 \pm 0.01$ ; Fig. 3b). The  $662.4$   
145  $\pm 3.9$  Ma Re-Os date for the Twitya Formation together with the CA-ID-TIMS zircon date  
146 of  $716.5 \pm 0.2$  Ma from the nearby Ogilvie Mountains (4) represents the first set of age  
147 constraints that date both the onset and demise of a Cryogenian glaciation from the same  
148 continental margin. Correlation of the Rapitan Group from the Yukon to the Northwest  
149 Territories (NWT) is supported not only by the bracketing stratigraphy, but also by the  
150 presence of iron formation (25, 26) and paleomagnetic studies that link Rapitan poles from  
151 the NWT with the 723–716 Ma Franklin large igneous province (20, 27), which was coeval  
152 with Rapitan glaciation in the Yukon (4).

153

#### 154 **Coupled Os and Sr Isotope Stratigraphy**

155 The Os and Sr isotope compositions of seawater have been interpreted to reflect an input  
156 balance between radiogenic sources (weathering of upper continental crust and riverine  
157 input) and unradiogenic sources (cosmic dust, hydrothermal alteration of oceanic crust and  
158 weathering of mafic or ultramafic rocks) (28). However, Os and Sr have distinct sources  
159 and sinks, are sensitive to varying geological processes and have contrasting residence  
160 times. Therefore, combining these two weathering proxies to investigate Neoproterozoic  
161 climatic fluctuations represents a novel method to elucidate the relationship between  
162 increased rates of continental weathering and global climate change.



163 Initial  $^{187}\text{Os}/^{188}\text{Os}$  ( $\text{Os}_i$ ) values from the pre-glacial Coppercap Formation become  
164 increasingly unradiogenic up-section from a value of 0.24 to a nadir of 0.12 prior to  
165 Rapitan Group deposition (Fig. 2). This extremely low  $\text{Os}_i$  value is substantially less  
166 radiogenic than values reported for modern seawater ( $^{187}\text{Os}/^{188}\text{Os} = 1.06$ ) (28) and is closer  
167 to the primitive upper mantle Os isotope composition (732 Ma =  $^{187}\text{Os}/^{188}\text{Os} = 0.124$ ) (29).  
168 Although it is possible that episodic restriction within the Coates Lake basin, potential  
169 hydrothermal input, and/or weathering of a proximal ultramafic body may have contributed  
170 to the unradiogenic  $\text{Os}_i$  values in the Coppercap Formation (Fig. 2), units CP2-CP6 have  
171 been previously interpreted to have been deposited in an open marine embayment (14, 30).

172 In the Coppercap Formation, Sr isotope values are extremely scattered in units CP1-  
173 CP3 between 0.7169 and 0.7064, less scattered in units CP4 and CP5 with values  
174 converging between 0.7064 and 0.7066, and scattered again in unit CP6. In the Twitya  
175 Formation, Sr isotope values decline from 0.7069 to 0.7067 in the basal 5 m and continue  
176 to oscillate between 0.7068 and 0.7070 over the ensuing 20 m (Fig. 2; Table S1).

177 Unlike the Phanerozoic marine Sr isotope curve, whose fidelity can be evaluated by  
178 comparisons between several sample types (31), Neoproterozoic marine Sr  
179 chemostratigraphy relies exclusively on analyses of whole rock carbonate samples that  
180 have potentially been subjected to a variety of diagenetic processes. Based on data from  
181 sequential dissolution experiments (32), Sr isotopic analyses of whole rock carbonate  
182 samples can be expected to vary in the fourth decimal place, i.e., the external  
183 reproducibility of “replicates” from the same sample is  $\pm 0.0001$ . Sr-isotope measurements  
184 are commonly vetted for reliability with Mn/Sr, Sr/Ca, Rb/Sr, and Sr concentration. Mn/Sr  
185 is thought to be a sensitive indicator of alteration due to the increase in Mn and decrease of

186 Sr during meteoric alteration (33, 34), however, we find that Mn/Sr and Rb/Sr ratios scale  
187 inversely with carbonate content (Table S1). This likely reflects the contamination of small  
188 amounts of Sr from clay. Consequently, we cull unreliable results with both low carbonate  
189 content and Sr abundance. Above 90% carbonate content and Sr concentrations >650 ppm,  
190  $^{87}\text{Sr}/^{86}\text{Sr}$  scatter above 0.708 is eliminated. However, there is no dependence on carbonate  
191 content and Sr concentration, or on Mn/Sr, Rb/Sr, or Sr/Ca on  $^{87}\text{Sr}/^{86}\text{Sr}$  between 0.7064 and  
192 0.7080 (Table S1). The lowest and most stratigraphically coherent and reproducible values  
193 are in units CP4 and CP5 and in the Twitya Formation. We thus consider these  $^{87}\text{Sr}/^{86}\text{Sr}$   
194 measurements as ‘most reliable’ (Fig. 2; Table S1).

195 The lower Coppercap Formation (units CP1-CP3) contains detrital components  
196 derived from the Little Dal Basalt and siliciclastic strata of the Katerine Group (14). These  
197 strata have also been geochemically modified by basin-dewatering brines that were  
198 responsible for formation of the Coates Lake sediment-hosted Cu deposit. We interpret the  
199 radiogenic  $^{87}\text{Sr}/^{86}\text{Sr}$  of the lower Coppercap Formation to reflect effects of both a higher  
200 clastic component, and post-depositional modification by basin-dewatering brines.

201

## 202 **Duration and Synchronicity of the Sturtian Glacial Epoch**

203 The Twitya Formation Re-Os date is identical, within uncertainty, to existing post-glacial  
204 U-Pb zircon geochronological data from Australia and South China (Fig. 4) (35, 36),  
205 although there are some discrepancies related to analytical procedures of some of the Re-Os  
206 ages from Australia (5, 6). Previous work yielded Re-Os age constraints for the Tindelpina  
207 Formation (6) which is an amalgamated date based on Re-Os data from two separate drill  
208 cores (SCYW-1a and Blinman-2) separated by >100 km. These two horizons were

209 correlated using low-resolution  $\delta^{13}\text{C}$  stratigraphy, not an accurate technique for sample  
210 selection for Re-Os geochronology. The 4-point SCYW1a isochron in their study (6)  
211 contains two data points (a3-4 and a3-4r; supplementary data of reference 6 and  
212 supplementary Table 5) that are actually two analyses of a single sample suggesting  
213 extreme sample heterogeneity. Due to these complications, we consider the SCYW1a age  
214 to be misleading and not provide meaningful geochronological data for global correlation.

215         A Re-Os date of  $640.7 \pm 4.7$  Ma from Tasmanian organic-rich rocks has also been  
216 used to dispute the synchronicity of the Rapitan-Sturtian deglaciation (5). However, this  
217 date from the upper Black River Formation is from a horizon located stratigraphically  
218 above two diamictite units that are separated by a carbonate unit, and is overlain by the ca.  
219 580 Ma Gaskiers-age Croles Hill diamictite (37). The Croles Hill diamictite was previously  
220 correlated with the Marinoan Cottons Breccia on King Island and the Elatina Formation in  
221 the Flinders Range of Australia, which implied that the upper Black River Formation was  
222 Sturtian in age. However, a new  $^{206}\text{Pb}/^{238}\text{U}$  zircon CA-ID-TIMS date of  $636.41 \pm 0.45$  Ma  
223 from the Cottons Breccia (23) suggests that the  $640.7 \pm 4.7$  Ma Re-Os age in the upper  
224 Black River Formation is instead correlative with the ca. 635 Ma Marinoan glaciation.

225         The glaciogenic Port Askaig Formation of the Dalradian Supergroup, Scotland was  
226 deposited on the NE margin of Laurentia and has been correlated with the Sturtian  
227 glaciation using lithostratigraphic and chemostratigraphic techniques (38, 39). A Re-Os age  
228 of  $659.6 \pm 9.6$  Ma for the Ballachulish Slate near Loch Leven (40) has been cited as a  
229 maximum age constraint for the Port Askaig Formation, however, the Port Askaig is not  
230 present in the region, and the relationship of the date to glaciogenic strata relies on regional  
231 correlations. The broad synchronicity of the Re-Os ages from the Ballachulish Slate

232 Formation and the Twitya Formation and the apparent disparity in their relationship to  
233 glaciogenic horizons calls into question the validity of these ages. A variety of tests on  
234 samples from the Ballachulish Slate indicate that the  $659.6 \pm 9.6$  Ma age represents a  
235 depositional age and not a mixed age from later metamorphic events (40). Therefore, if we  
236 assume that the ages on the Ballachulish and Twitya formations are robust, we are left with  
237 the following alternatives: 1) these dates are constraining two separate glaciations during  
238 the “Sturtian glacial epoch,” and these ages bracket the later event, 2) the Sturtian  
239 glaciation is not preserved on the eastern margin of Laurentia and the Port Askaig  
240 Formation represents the younger ( $\sim 635$  Ma) Marinoan glaciation and is correlative with  
241 the Stralinchy diamictite, or 3) the Kinlochlaggan Boulder Bed is correlative with the Port  
242 Askaig Tillite as originally suggested by (41, 42), and as a result, the Ballachulish Slate  
243 near Loch Leven would lie in the Argyll Group. Ultimately, additional tests of regional  
244 correlations and geochronological constraints are necessary to more fully resolve the  
245 complexities of the Dalradian Supergroup.

246 Existing  $^{206}\text{Pb}/^{238}\text{U}$  zircon ages from Idaho have been previously used to argue that  
247 the Sturtian glaciation is globally diachronous (43, 44). However, these ages, coupled with  
248 the  $711.5 \pm 0.3$  Ma age from the Gubrah Formation in Oman (45), can also be interpreted to  
249 be syn-glacial constraints and correlative with the 717–662 Ma Sturtian glacial epoch  
250 recorded in NW Canada (Fig. 4). Additional constraints from U-Pb and Re-Os  
251 geochronology are necessary to determine if Sturtian glacial strata represent a series of  
252 glacial-interglacial cycles (46), a Jormagund climate state (47), or a continuous  $\sim 55$  Myr  
253 Snowball Earth event.

254 It has also been suggested that there was an earlier, ca. 750 Ma glaciation recorded  
255 on the Kalahari (48), Congo (49), and Tarim (50) cratons. However, there is no direct  
256 evidence for glaciation in Kaigas Formation on the Kalahari Craton (51), and the ages from  
257 the Congo and Tarim cratons suffer from inheritance and cannot be relied on (see concordia  
258 diagrams in references 49 and 50). Our Re-Os age of  $732.2 \pm 3.9$  Ma on the Coppercap  
259 Formation coupled with global C and Sr isotope correlation is further consistent with the  
260 lack of evidence for a pre-717 Ma glaciation. The large negative carbon isotope anomaly in  
261 the lower Coppercap Formation covaries in carbonate carbon and organic carbon isotopes  
262 (Fig. 2) and can be correlated with the Islay anomaly in Scotland, Greenland, and Svalbard  
263 (3), consistent with pre-Sturtian Sr isotope values (52, 53). However, the Islay anomaly in  
264 Scotland is not present in the Loch Leven region in Scotland and its relationship to the  
265 dated Ballachulish Slate (40) is unclear. The Re-Os geochronology presented here suggests  
266 that the Islay anomaly returns to positive  $\delta^{13}\text{C}_{\text{carb}}$  values by  $\sim 732$  Ma, well before the onset  
267 of glaciation at  $\sim 717$  Ma (4) and thus cannot be mechanistically linked to the onset of  
268 glaciation as has been previously proposed (54-56). Moreover, none of these successions  
269 host any evidence for glaciation prior to the Islay anomaly.

270

## 271 **Fire and Ice Revisited**

272 The Sr isotope data reported here at ca. 732 Ma – as low as  $\sim 0.7064$  in the Coppercap  
273 Formation – are consistent with other low pre-Sturtian values recorded in strata from  
274 Svalbard and Greenland (52, 53) and are less radiogenic than the ca. 780 Ma values from  
275 Svalbard (57). Interestingly, Nd isotope studies have also suggested an increase to more  
276 mantle-like (more radiogenic) values tens of millions of years prior to the Sturtian

277 glaciation (57). These data are consistent with the ‘Fire and Ice’ hypothesis (58, 59), which  
278 proposes that Cryogenian glaciations were initiated through enhanced CO<sub>2</sub> consumption via  
279 weathering of basalts emplaced at low-latitudes. The low-latitude breakup of Rodinia is  
280 thought to have been associated with the development of multiple juvenile volcanic rift  
281 margins and the emplacement of multiple large igneous provinces (e.g., Willouran, Guibei,  
282 Gunbarrel, and Franklin LIPs) (60). Enhanced volcanism and weathering of mafic material  
283 would have driven the ocean towards more unradiogenic Sr values and mantle-like Os<sub>i</sub>  
284 values and a cooler global climate (Fig. 4), analogous to scenarios proposed for Mesozoic  
285 ocean anoxic events and Cenozoic cooling episodes (61-63).

286 In sharp contrast, the Os<sub>i</sub> data from the overlying Twitya Formation yield a  
287 radiogenic signal for the post-glacial ocean with the basal cap limestone recording an Os<sub>i</sub>  
288 value of 1.44. From this initial high, values decline rapidly reaching a nadir of 0.42 at a  
289 height 2.6 m above the diamictite, then become steadily more radiogenic to a value of 0.62  
290 before stabilizing to values ~0.50 above 10 m (Fig. 2). Similarly, Sr isotope values decrease  
291 from 0.7068 to 0.7066 in the lower 3 m and continue to fluctuate up section to before  
292 levelling out between 0.7068 and 0.7070. We interpret the signal recorded in the lower 3 m  
293 to represent the highly radiogenic, unmixed glacial melt water plume (64) and a subsequent  
294 decrease to less radiogenic Sr isotope values at 3–10 m to reflect the transgression of  
295 glacial deep waters (65). Up-section, it appears as though rapid mixing obscures the melt  
296 water signal; however, enhanced silicate weathering continued through the transgression in  
297 a high *p*CO<sub>2</sub> environment, resulting in an Os<sub>i</sub> much more radiogenic than pre-glacial values  
298 that complement the radiogenic trend recorded in the coeval Sr composition of seawater  
299 (Fig. 2). The absence of a trend to unradiogenic Sr isotope values across Cryogenian glacial

300 deposits led some workers to conclude that Neoproterozoic glaciations were short-lived (<1  
301 Myr) (66). However, this approach neglects carbonate dissolution in response to ocean  
302 acidification and assumes that the Sr cycle is in steady state (67, 68), which is inconsistent  
303 with the sharp rise seen in globally distributed cap carbonate deposits.

304 Sr isotope data from Sturtian cap limestones in Namibia, Mongolia, and NW  
305 Canada agree to the fourth decimal place (69,70) thereby supporting a global correlation of  
306 this trend (Fig. 5). These Sr values increase rapidly from 0.7066 to 0.7072 in the Sturtian  
307 cap carbonate sequence and then flat-line through the rest of the Cryogenian period. Thus,  
308 the Neoproterozoic rise in seawater Sr isotope values may not have been gradual, as  
309 previously suggested (52), but stepwise and driven by extreme weathering in a post-glacial  
310 super-greenhouse.

311

## 312 **Conclusions**

313 The geological record suggests that the Earth's climate system can exist in two climatic  
314 equilibria, one globally glaciated and the other not (46, 47). However, both the processes  
315 that maintain a steady climate and the drivers of long-term (>10 Myr) climate change have  
316 remained obscure. Following a billion years of relative climatic stability with no apparent  
317 glacial deposits, the Neoproterozoic witnessed the transition from an ice-free world to a  
318 Snowball Earth. The new Os and Sr isotope stratigraphy coupled with the Re-Os  
319 geochronology data presented herein also point towards a tectonic driver for long-term  
320 climate change and that the change in global weatherability may have been driven by a  
321 relative increase in juvenile, mantle-derived material weathered into the oceans from the  
322 continents.

323 Initiation of a Snowball Earth through a change in global weatherability has been  
324 criticized on the grounds that these background conditions should have persisted on >10  
325 Myr timescale and after deglaciation the Earth should have rapidly returned to a Snowball  
326 state (46). Our new constraint of a ~55 Myr duration of the Sturtian glacial epoch in NW  
327 Canada is consistent with a short interlude between the Sturtian and Marinoan glaciations  
328 and a return to a glacial state on a timescale consistent with enhanced weatherability (71).  
329 Enhanced input of mantle-derived material to the ocean would have also influenced  
330 geochemical cycles and promoted anaerobic respiration, potentially providing additional  
331 feedbacks that conspired to initiate a Neoproterozoic Snowball Earth (54). Our results  
332 confirm that the Sturtian glacial epoch was long lasting, its onset was accompanied by  
333 basalt-dominated weathering, and its termination was globally synchronous and followed  
334 by extreme weathering of the continents. The post-Sturtian weathering event may have in  
335 turn provided limiting nutrients like phosphorous to the ocean (72), leading to an increase  
336 in atmospheric oxygen and the radiation of large animals with high metabolic demands.

337

338 **ACKNOWLEDGMENTS.** We thank Rigel Lustwerk for providing samples from the 6YR core. We are grateful  
339 to the Yukon Geological Survey, Roger Summons and MIT's NAI astrobiology node for support. We thank  
340 Roger Summons, Sam Bowring and Dan Schrag for the use of their labs. The Durham Laboratory for Source  
341 Rock Geochronology and Geochemistry is partially funded by TOTAL and BP. CH was supported by the  
342 Agouron Institute. We wish to acknowledge the superb teams at Canadian and Fireweed helicopter companies  
343 and Dugald Dunlop from Meridian Mining via Colorado Minerals. We thank three reviewers and Paul  
344 Hoffman for comments on the manuscript and editorial advice.

345

346 1. Hoffman PF, Kaufman AJ, Halverson GP, & Schrag DP (1998) A Neoproterozoic  
347 Snowball Earth. *Science* 281:1342-1346.



- 348 2. Hoffman PF & Schrag DP (2002) The snowball Earth hypothesis; testing the limits of  
349 global change. *Terra Nova* 14(3):129-155.
- 350 3. Halverson GP, Hoffman PF, Schrag DP, Maloof AC, & Rice AHN (2005) Toward a  
351 Neoproterozoic composite carbon-isotope record. *Geological Society of America*  
352 *Bulletin* 117(9-10):1181-1207.
- 353 4. Macdonald FA, *et al.* (2010) Calibrating the Cryogenian. *Science* 327:1241-1243.
- 354 5. Kendall BS, Creaser RA, Calver CR, Raub TD, & Evans DAD (2009) Correlation of  
355 Sturtian diamictite successions in southern Australian and northwestern Tasmania by  
356 Re-Os black shale geochronology and the ambiguity of "Sturtian"-type diamictite-cap  
357 carbonate pairs as chronostratigraphic marker horizons. *Precambrian Research*  
358 172:301-310.
- 359 6. Kendall BS, Creaser RA, & Selby D (2006) Re-Os geochronology of postglacial  
360 black shales in Australia: constraints on the timing of "Sturtian" glaciation. *Geology*  
361 34:729-732.
- 362 7. Ravizza G & Peucker-Ehrenbrink B (2003) The marine  $^{187}\text{Os}/^{188}\text{Os}$  record of the  
363 Eocene-Oligocene transition: the interplay of weathering and glaciation. *Earth and*  
364 *Planetary Science Letters* 210:151-165.
- 365 8. Raymo ME & Ruddiman WF (1992) Tectonic forcing of late Cenozoic climate.  
366 *Nature* 359:117-122.
- 367 9. Paquay FS & Ravizza G (2012) Heterogeneous seawater  $^{187}\text{Os}/^{188}\text{Os}$  during the Late  
368 Pleistocene glaciations. *Earth and Planetary Science Letters* 349:126-138.
- 369 10. Dudás FO & Lustwerk RL (1997) Geochemistry of the Little Dal basalts: continental  
370 tholeiites from the Mackenzie Mountains, Northwest Territories, Canada. *Canadian*  
371 *Journal of Earth Sciences* 34:50-58.
- 372 11. Jefferson CW & Parrish R (1989) Late Proterozoic stratigraphy, U/Pb zircon ages and  
373 rift tectonics, Mackenzie Mountains, northwestern Canada. *Canadian Journal of*  
374 *Earth Sciences* 26:1784-1801.
- 375 12. Harlan SS, Heaman LM, LeCheminant AN, & Premo WR (2003) Gunbarrel mafic  
376 magmatic event: a key 780 Ma time marker for Rodinia plate reconstructions.  
377 *Geology* 31:1053-1056.
- 378 13. Chartrand FM & Brown AC (1985) The diagenetic origin of stratiform copper  
379 mineralization, Coates Lake, Redstone Copper belt, NWT, Canada. *Economic*  
380 *Geology* 80:325-343.
- 381 14. Lustwerk RL (1990) Geology and geochemistry of the Redstone strataform copper  
382 deposit, Northwest Territories, Canada. PhD (Pennsylvania State University).
- 383 15. Helmstaedt H, Eisbacher GH, & McGregor JA (1979) Copper mineralization near an  
384 intra-Rapitan unconformity, Nite copper prospect, Mackenzie Mountains, Northwest  
385 Territories, Canada. *Canadian Journal of Earth Sciences* 16:50-59.
- 386 16. Eisbacher GH (1978) Redefinition and subdivision of the Rapitan Group, Mackenzie  
387 Mountains. *Geological Survey of Canada Paper* 77-35:1-21.
- 388 17. Hoffman PF & Halverson GP (2011) Neoproterozoic glacial record in the Mackenzie  
389 Mountains, northern Canadian Cordillera. *The Geological Record of Neoproterozoic*  
390 *Glaciations*, eds Arnaud E, Halverson GP, & Shields-Zhou G (The Geological  
391 Society, London), Vol 36, pp 397-412.

- 392 18. Klein C & Beukes NJ (1993) Sedimentology and geochemistry of the glaciogenic late  
393 Proterozoic Rapitan iron-formation in Canada. *Economic Geology* 84:1733-1774.
- 394 19. Eisbacher GH (Sedimentary tectonics and glacial record in the Windermere  
395 Supergroup, Mackenzie Mountains, northwestern Canada. Geological Survey of  
396 Canada Paper 80-27, pp 1-40.
- 397 20. Park JK (1997) Paleomagnetic evidence for low-latitude glaciation during deposition  
398 of the Neoproterozoic Rapitan Group, Mackenzie Mountains, N.W.T., Canada.  
399 *Canadian Journal of Earth Sciences* 34:34-49.
- 400 21. Aitken JD (1991) The Ice Brook Formation and Post-Rapitan, Late Proterozoic  
401 glaciation, Mackenzie Mountains, Northwest Territories. *Geological Survey of*  
402 *Canada Bulletin* 404:1-43.
- 403 22. James NP, Narbonne GM, & Kyser TK (2001) Late Neoproterozoic cap carbonates:  
404 Mackenzie Mountains, northwestern Canada: precipitation and global glacial  
405 meltdown. *Canadian Journal of Earth Sciences* 38(8):1229-1262.
- 406 23. Calver CR, *et al.* (2013) Globally synchronous Marinoan deglaciation indicated by U-  
407 Pb geochronology of the Cottons Breccia, Tasmania, Australia. *Geology* 41:1127-  
408 1130.
- 409 24. Johnston DT, Macdonald FA, Gill B, Hoffman PF, & Schrag DP (2012) Uncovering  
410 the Neoproterozoic carbon cycle. *Nature* 483(7389):320-323.
- 411 25. Young GM (1976) Iron-formation and glaciogenic rocks of the Rapitan Group,  
412 Northwest Territories, Canada. *Precambrian Research* 3:137-158.
- 413 26. Young GM (1982) The late Proterozoic Tindir Group, east-central Alaska; Evolution  
414 of a continental margin. *Geological Society of America Bulletin* 93:759-783.
- 415 27. Denyszyn SW, Halls HC, Davis DW, & Evans DAD (2009) Paleomagnetism and U-  
416 Pb geochronology of Franklin dykes in High Arctic Canada and Greenland: a revised  
417 age and paleomagnetic pole for constraining block rotations in the Nares Strait region.  
418 *Canadian Journal of Earth Sciences* 46:689-705.
- 419 28. Peucker-Ehrenbrink B & Ravizza G (2000) The marine osmium isotope record. *Terra*  
420 *Nova* 12:205-219.
- 421 29. Meisel T, Walker RJ, Irving AJ, & Lorand J-P (2001) Osmium isotopic compositions  
422 of mantle xenoliths: a global perspective. *Geochimica et Cosmochimica Acta*  
423 65:1311-1323.
- 424 30. Jefferson CW (1978) The Upper Proterozoic Redstone Copper Belt, Mackenzie  
425 Mountains, Northwest Territories. Ph.D (University of Western Ontario, London).
- 426 31. Brand U (2004) Carbon, oxygen and strontium isotopes in Paleozoic carbonate  
427 components: an evaluation of original seawater-chemistry proxies. *Chemical Geology*  
428 204:23-44.
- 429 32. Li D, Shields-Zhou G, Ling HF, & Thirwall M (2011) Dissolution methods for  
430 strontium isotope stratigraphy: Guidelines for the use of bulk carbonate and  
431 phosphorite rocks. *Chemical Geology* 290:133-144.
- 432 33. Derry LA, Keto LS, Jacobsen SB, Knoll AH, & Swett K (1989) Sr isotopic variations  
433 in Upper Proterozoic carbonates from Svalbard and East Greenland. *Geochimica et*  
434 *Cosmochimica Acta* 53(9):2231-2339.

- 435 34. Banner JL & Hanson GN (1990) Calculation of simultaneous isotopic and trace  
436 element variations during water-rock interaction with application to carbonate  
437 diagenesis. *Geochimica et Cosmochimica Acta* 54:3123-3137.
- 438 35. Fanning CM & Link PK (2008) Age constraints for the Sturtian glaciation: data from  
439 the Adelaide Geosyncline, South Australia and Pocatello Formation Idaho, USA.  
440 *Geological Society of Australia Abstracts, No. 91, Selwyn Symposium 2008,*  
441 *Melbourne:57-62.*
- 442 36. Zhou C, *et al.* (2004) New constraints on the ages of Neoproterozoic glaciations in  
443 south China. *Geology* 32:437-440.
- 444 37. Calver CR, Black LP, Everard JL, & Seymour DB (2004) U-Pb zircon age constraints  
445 on late Neoproterozoic glaciation in Tasmania. *Geology* 32(10):893-896.
- 446 38. Brasier MD & Shields G (2000) Neoproterozoic chemostratigraphy and correlation of  
447 the Port Askaig glaciation, Dalradian Supergroup of Scotland. *Journal of the*  
448 *Geological Society of London* 157:909-914.
- 449 39. Prave AR, Fallick AE, Thomas CW, & Graham CM (2009) A composite C-isotope  
450 profile for the Neoproterozoic Dalradian Supergroup of Scotland and Ireland. *Journal*  
451 *of the Geological Society of London* 166:1-13.
- 452 40. Rooney AD, Chew DM, & Selby D (2011) Re-Os geochronology of the  
453 Neoproterozoic-Cambrian Dalradian Supergroup of Scotland and Ireland:  
454 implications for Neoproterozoic stratigraphy, glaciation and Re-Os systematics.  
455 *Precambrian Research* 185:202-214.
- 456 41. Treagus JE (1969) The Lower Dalradian Kinlochlaggan Boulder Bed, central  
457 Scotland. *Earth pre-Pleistocene glacial record*, eds Hambrey MJ & Harland WB  
458 (Cambridge University Press, Cambridge, UK), pp 637-639.
- 459 42. Evans RHS & Tanner PWG (1996) A late Vendian age for the Kinlochlaggan Boulder  
460 Bed (Dalradian)? *Journal of the Geological Society, London* 153:823-826.
- 461 43. Fanning CM & Link PK (2004) U-Pb SHRIMP ages of Neoproterozoic (Sturtian)  
462 glaciogenic Pocatello Formation, southeastern Idaho. *Geology* 32:881-884.
- 463 44. Keeley JA, Link PK, Fanning CM, & Schmitz MD (2013) Pre- to synglacial rift-  
464 related volcanism in the Neoproterozoic (Cryogenian) Pocatello Formation, SE Idaho:  
465 New SHRIMP and CA-ID-TIMS constraints. *Lithosphere* 5(1):128-150.
- 466 45. Bowring SA, Grotzinger JP, Condon DJ, Ramezani J, & Newall M (2007)  
467 Geochronologic constraints on the chronostratigraphic framework of the  
468 Neoproterozoic Huqf Supergroup, Sultanate of Oman. *American Journal of Science*  
469 307:1097-1145.
- 470 46. Pierrehumbert RT, Abbot DS, Voigt A, & Koll D (2011) Climate of the  
471 Neoproterozoic. *Annual Review of Earth and Planetary Sciences* 39:417-460.
- 472 47. Abbot DS, Voigt A, & Koll D (2011) The Jormungand global climate state and  
473 implications for Neoproterozoic glaciations. *Journal of Geophysical Research*  
474 116(D18103).
- 475 48. Frimmel HE, Klotzli US, & Siegfried PR (1996) New Pb-Pb single zircon age  
476 constraints on the timing of Neoproterozoic glaciation and continental break-up in  
477 Namibia. *Journal of Geology* 104:459-469.
- 478 49. Key RM, *et al.* (2001) The western arm of the Lufilian Arc in NW Zambia and its  
479 potential for copper mineralization. *Journal of African Earth Sciences* 33:503-528.

- 480 50. Xu B, *et al.* (2009) SHRIMP zircon U-Pb age constraints on Neoproterozoic  
481 Quruqtagh diamictites in NW China. *Precambrian Research* 168:247-258.
- 482 51. Macdonald FA, Strauss JV, Rose CV, Dudás FO, & Schrag DP (2010) Stratigraphy of  
483 the Port Nolloth Group of Namibia and South Africa and implications for the age of  
484 Neoproterozoic iron formations. *American Journal of Science* 310:862-888.
- 485 52. Halverson GP, Dudás FO, Maloof AC, & Bowring SA (2007) Evolution of the  
486  $^{87}\text{Sr}/^{86}\text{Sr}$  composition of Neoproterozoic seawater. *Palaeogeography*  
487 *Palaeoclimatology Palaeoecology* 256:103-129.
- 488 53. Fairchild IJ, Spiro B, Herrington PM, & Song T (2000) Controls on Sr and C isotope  
489 compositions of Neoproterozoic Sr-rich limestones of East Greenland and North  
490 China. *Carbonate Sedimentation and Diagenesis in the Evolving Precambrian World*,  
491 eds Grotzinger JP & James NP (SEPM Special Publication, Tulsa), Vol 67, pp 297-  
492 313.
- 493 54. Tziperman E, Halevy I, Johnston DT, Knoll AH, & Schrag DP (2011) Biologically  
494 induced initiation of Neoproterozoic snowball-Earth events. *Proceedings of the*  
495 *National Academy of Sciences* 108(108):15091-15096.
- 496 55. Hoffman PF, *et al.* (2012) Cryogenian glaciations on the southern tropical  
497 paleomargin of Laurentia (NE Svalbard and East Greenland), and a primary origin for  
498 the upper Russoya (Islay) carbon isotope excursion. *Precambrian Research* 206-  
499 207:137-158.
- 500 56. Schrag DP, Berner RA, Hoffman PF, & Halverson GP (2002) On the initiation of  
501 snowball Earth. *Geochemistry, Geophysics, Geosystems* 3.
- 502 57. Halverson GP, Wade BP, Hurtgen MT, & Barovich KM (2010) Neoproterozoic  
503 Chemostratigraphy. *Precambrian Research* 182(4):337-350.
- 504 58. Donnadieu Y, Godderis Y, Ramstein G, Nedelec A, & Meert J (2004) A 'snowball  
505 Earth' climate triggered by continental break-up through changes in runoff. *Nature*  
506 428:303-306.
- 507 59. Godderis Y, *et al.* (2003) The Sturtian 'snowball' glaciation: fire and ice. *Earth and*  
508 *Planetary Science Letters* 6648:1-12.
- 509 60. Li ZX, *et al.* (2008) Assembly, configuration, and break-up history of Rodinia: A  
510 synthesis. *Precambrian Research* 160(1-2):179-210.
- 511 61. Ravizza G & Peucker-Ehrenbrink B (2003) Chemostratigraphic evidence of Deccan  
512 volcanism from the marine osmium isotope record. *Science* 302:1392-1395.
- 513 62. Turgeon SC & Creaser RA (2008) Cretaceous oceanic anoxia event 2 triggered by a  
514 massive magmatic episode. *Nature* 454:323-327.
- 515 63. Kent DV & Muttoni G (2013) Modulation of Late Cretaceous and Cenozoic climate  
516 by variable drawdown of atmospheric  $p\text{CO}_2$  from weathering of basaltic provinces on  
517 continents drifting through the equatorial humid belt. *Climates of the Past*. 9: 525-  
518 546.
- 519 64. Shields G (2005) Neoproterozoic cap carbonates: a critical appraisal of existing  
520 models and the plumeworld hypothesis. *Terra Nova* 17(4):299-310.
- 521 65. Hoffman PF, *et al.* (2007) Are basal Ediacaran (635 Ma) post-glacial "cap  
522 dolostones" diachronous? *Earth and Planetary Science Letters* 258:114-131.
- 523 66. Jacobsen S & Kaufman AJ (1999) The Sr, C, and O isotopic evolution of  
524 Neoproterozoic seawater. *Chemical Geology* 161:37-57.

- 525 67. Le Hir G, Ramstein G, Donnadieu Y, & Godderis Y (2008) Scenario for the evolution  
526 of atmospheric pCO<sub>2</sub> during a snowball Earth. *Geology* 36:47-50.
- 527 68. Higgins JA & Schrag DP (2003) Aftermath of a snowball Earth. *Geophysics,*  
528 *Geochemistry, Geosystems* 4:1-20.
- 529 69. Yoshioka H, Asahara Y, Tojo B, & Kawakami S (2003) Systematic variations in C  
530 and Sr isotopes and elemental concentrations in Neoproterozoic carbonates in  
531 Namibia: implications for a glacial to interglacial transition. *Precambrian Research*  
532 124:69-85.
- 533 70. Shields G, Brasier MD, Stille P, & Dorjnamjaa D (2002) Factors contributing to high  
534  $\delta^{13}\text{C}$  values in Cryogenian limestones of western Mongolia. *Earth and Planetary*  
535 *Science Letters* 196:99-111.
- 536 71. Mills B, Watson AJ, Goldblatt C, Boyle RA, & Lenton TM (2011) Timing of  
537 Neoproterozoic glaciations linked to transport-limited global weathering. *Nature*  
538 *Geoscience* 4:861-864.
- 539 72. Planavsky NJ, *et al.* (2010) The evolution of the marine phosphate reservoir. *Nature*  
540 467:1088-1090.

541

542

543 **Figure Legends.**

544 **Fig. 1.** Schematic stratigraphy of Tonian, Cryogenian and Ediacaran strata of the  
545 Mackenzie and Ogilvie Mountains. U-Pb ages are from ref. (4) and Re-Os ages are from  
546 this work (Reefal Ass, Reefal Assemblage; Mt, Mount; V.C., volcanic complex; Congl.,  
547 conglomerate; Coates Lk, Coates Lake; Thund., Thundercloud Formation; Cu-cap,  
548 Coppercap Formation).

549

550 **Fig. 2.** Composite chemo- and lithostratigraphy of the Windermere Supergroup from the  
551 Mackenzie Mountains, Canada (measured sections F1173, P5C and 6YR). Organic carbon  
552 isotope data for the Twitya Formation in Section P5C is from (24) (Say, Sayunei; Sh,  
553 Shezal). The superscript next to 716 and 717 Ma corresponds to the cited reference.

554

555 **Fig. 3.** (A) Re-Os isochron for the Coppercap Formation with an age uncertainty of 4.7 Ma  
556 when the uncertainty in the  $^{187}\text{Re}$  decay constant is included. (B) Re-Os isochron for the  
557 Twitya Formation with an age uncertainty of 4.6 Ma when the uncertainty in the  $^{187}\text{Re}$   
558 decay constant is included. Isotope composition and abundance data are presented in Table  
559 S2.

560

561 **Fig. 4.** (A) Compilation of initial  $^{187}\text{Os}/^{188}\text{Os}$  isotope data and  $^{87}\text{Sr}/^{86}\text{Sr}$  data for pre- and  
562 post-Sturtian successions worldwide (5, 6, 40, 53, 70). All data are in Tables S1-5. (B)  
563 Geological cartoon of Neoproterozoic pre-glacial weathering fluxes. (C) Geological cartoon  
564 of post-glacial weathering fluxes. See text and SI for further details.

Supplementary Table 1: TOC, carbon, strontium, oxygen isotope and trace element data for sections of Coppercap and Twitya formations.

Rapitan	Sample	Height in m (from base of CC)	Lithology	TOC (wt %)	$\delta^{13}\text{C}_{\text{carb}}$ ‰ (VPDB)	$\delta^{18}\text{O}$ ‰ (VPDB)	$^{87}\text{Sr}/^{86}\text{Sr}$	$\delta^{13}\text{C}_{\text{org}}$ ‰ (VPDB)	C Epsilon ‰	Sr (ppm)	Mn (ppm)	Mn/Sr	% CARB	Rb/Sr	Mg/Ca
6YR	76	421.2	gy gs wacke	0.02	2.70	-10.95	0.71021	-36.39	39.09	-	-	-	-	-	-
6YR	77	416.7	diamictite	-	3.68	-10.35	0.71050	-	-	704	4486	6.372	24.7	0.0240	0.07866
6YR	78	416.6	gy microbial	-	4.43	-10.79	0.70987	-	-	344	1404	4.080	81.4	0.0101	0.06254
6YR	79	413.7	gy gs	0.01	3.65	-8.64	0.70981	-37.02	40.67	366	1232	3.365	54.3	0.0052	0.18743
6YR	80	408.2	gy micrite	0.01	5.70	-11.45	0.70841	-25.72	31.42	295	102	0.345	100.1	0.0021	0.00726
6YR	81	405.2	wht brecc dol	-	6.10	-15.15	0.70762	-	-	204	152	0.746	81.5	0.0023	0.00338
6YR	82	402.4	wht brecc dol	-	6.08	-15.88	0.70714	-	-	-	-	-	-	-	-
6YR	83	396.7	wht brecc dol	-	-7.30	-6.41	0.70662	-	-	-	-	-	-	-	-
6YR	84	393.5	dgy gs wacke	0.03	3.69	-4.37	0.70665	-22.83	26.53	1428	83	0.058	82.5	0.0006	0.18079
6YR	85	379.9	dgy micrite	0.04	6.28	-2.60	0.70667	-20.96	27.24	1583	50	0.032	76.9	0.0003	0.60862
6YR	86	376.0	dgy micrite	-	5.35	-4.13	0.70668	-	-	1957	74	0.038	80.5	0.0003	0.19336
6YR	87	374.7	gy gs	0.01	6.72	-4.43	0.70667	-26.89	33.61	-	-	-	-	-	-
6YR	88	368.9	gy gs	-	6.46	-5.26	0.70665	-	-	1866	95	0.051	68.4	0.0002	0.18952
6YR	89	363.4	gy gs, ev	0.07	5.76	-4.90	0.70657	-31.03	36.79	-	-	-	-	-	-
6YR	90	358.2	dgy micrite	-	5.72	-5.12	0.70664	-	-	1489	374	0.251	95.6	0.0003	0.03695
6YR	91	353.1	dgy micrite	0.04	7.04	-7.05	0.70653	-18.04	25.09	695	40	0.058	101.1	0.0005	0.00788
6YR	92	347.2	dgy micrite	0.09	5.30	-5.45	0.70667	-22.38	27.67	902	173	0.192	98.0	0.0007	0.05230
6YR	93	341.8	dgy micrite	-	5.08	-5.63	0.70666	-	-	973	118	0.121	98.3	0.0011	0.09666
6YR	94	337.2	dgy micrite	-	6.53	-3.93	0.70651	-	-	807	51	0.063	99.9	0.0005	0.00909
6YR	95	331.2	dgy micrite	0.08	6.59	-3.66	0.70649	-20.53	27.12	1117	51	0.046	93.9	0.0003	0.00895
6YR	96	325.5	dgy microbial	-	6.33	-3.52	0.70650	-	-	1267	74	0.058	98.1	0.0009	0.01123
6YR	97	321.2	dgy micrite	0.08	6.15	-4.33	0.70648	-20.55	26.70	1016	70	0.068	98.8	0.0004	0.01024
6YR	98	315.2	dgy gs wacke	-	4.95	-4.13	0.70650	-	-	1355	109	0.080	98.3	0.0006	0.01337
6YR	99	311.7	dgy micrite	0.06	4.72	-4.44	0.70648	-22.54	27.26	982	59	0.060	99.9	0.0004	0.01807
6YR	100	305.2	dgy gs	0.05	3.30	-5.30	0.70659	-25.65	28.95	1205	67	0.056	98.7	0.0003	0.02124
6YR	101	299.2	gy gs	0.11	4.42	-4.27	0.70660	-25.88	30.30	2048	99	0.048	86.9	0.0012	0.04859
6YR	102	292.0	dgy micrite	0.23	2.64	-3.53	0.70668	-24.16	26.80	1148	709	0.618	50.2	0.0081	0.41265
6YR	103	284.2	dgy gs	-	2.48	-3.74	0.70674	-	-	1166	157	0.134	50.7	0.0023	0.12620
6YR	104	277.2	dgy micrite	0.23	2.98	-4.04	0.70669	-25.82	28.80	828	144	0.175	89.8	0.0035	0.14382

6YR	105	268.7	dgy micrite	0.48	2.00	-3.98	0.70691	-26.92	28.92	1189	103	0.086	89.7	0.0017	0.05358
6YR	106	262.6	dgy micrite	0.36	0.41	-2.79	0.70713	-25.67	26.08	772	347	0.449	83.3	0.0056	0.53384
6YR	107	255.2	dgy micrite	-	0.71	-4.36	0.70704	-	-	1187	104	0.088	59.1	0.0022	0.10019
6YR	108	249.9	gy gs	0.08	0.71	-6.76	0.70706	-29.31	30.02	1142	25	0.022	84.3	0.0012	0.05783
6YR	109	242.8	gy gs	-	-1.53	-5.30	0.70683	-	-	1699	115	0.068	94.3	0.0005	0.55264
6YR	110	235.7	gy gs	0.03	0.29	-3.77	0.70691	-28.75	29.04	1446	96	0.067	60.1	0.0005	0.58983
6YR	111	229.8	dgy gs	-	0.09	-4.73	0.70751	-	-	684	68	0.099	50.2	0.0011	0.11193
6YR	112	222.5	gy microbial	0.57	-0.86	-5.94	0.70781	-30.06	29.20	-	-	-	-	-	-
6YR	113	217.0	gy gs	0.30	-2.37	-2.90	0.71107	-31.16	28.79	251	720	2.872	95.1	0.0574	0.67578
6YR	114	208.5	dgy micrite	0.45	-3.39	-6.92	0.70939	-33.38	29.99	-	-	-	-	-	-
6YR	115	201.8	dgy microbial	0.08	-2.19	-4.85	0.71457	-28.87	26.67	-	-	-	-	-	-
6YR	116	194.8	dgy micrite	-	-4.54	-3.77	0.70969	-	-	287	1184	4.119	42.3	0.0310	0.66623
6YR	117	188.2	dgy micrite	1.39	-4.29	-5.58	0.70644	-31.88	27.59	327	824	2.523	51.5	0.0313	0.32804
6YR	118	180.7	dgy micrite	0.17	-5.32	-7.07	0.71280	-30.94	25.62	714	709	0.992	15.1	0.0043	0.06225
6YR	119	173.2	dgy micrite	-	-3.28	-4.66	0.71352	-	-	-	-	-	-	-	-
6YR	120	168.1	dgy wacke	0.11	-5.02	-6.20	0.70787	-32.34	27.32	888	1110	1.249	57.2	0.0015	0.21395
6YR	122	152.5	dgy micrite	-	-4.87	-4.90	0.71289	-	-	198	1788	9.037	61.1	0.0462	0.77903
6YR	123	145.1	dgy micrite	0.17	-4.94	-5.58	0.71324	-31.80	26.86	-	-	-	-	-	-
6YR	125	97.5	gy micrite	0.11	-6.09	-6.17	0.71266	-32.05	25.96	341	1514	4.441		0.0810	0.31223
6YR	128	99.4	gy micrite	0.26	-4.42	-4.70	0.71688	-31.97	27.55	157	1652	10.508	37.3	0.0741	0.60216
6YR	129	124.1	gy micrite	0.09	-3.65	-5.01	0.71550	-31.48	27.83	636	179	0.281	79.3	0.0038	0.08526
6YR	130	131.2	gy micrite	0.11	-5.10	-4.74	0.71178	-31.49	26.39	-	-	-	27.2	-	-

Twitya	Sample	Height in m (from contact with Shezal)	Lithology	TOC (wt %)	$\delta^{13}\text{C}_{\text{carb}}$ ‰ (VPDB)	$\delta^{18}\text{O}$ ‰ (VPDB)	$^{87}\text{Sr}/^{86}\text{Sr}$	$\delta^{13}\text{C}_{\text{org}}$ ‰ (VPDB)	C Epsilon ‰	Sr (ppm)	Mn (ppm)	Mn/Sr	% CARB	Rb/Sr	Mg/Ca
F1173	0.1	0.1	dgy lime micrite	-	-2.10	-8.40	0.70693	-	-	641	468	0.701	96.1	-	0.01235
F1173	0.5	0.5	dgy lime micrite	-	-2.69	-8.66	0.70751	-	-	-	-	-	-	-	-
F1173	1.0	1.0	dgy lime micrite	-	-2.47	-8.56	0.70690	-	-	-	-	-	-	-	-
F1173	1.6	1.6	dgy lime micrite	-	-0.95	-8.89	0.70686	-	-	-	-	-	-	-	-
F1173	2.0	2.0	dgy lime micrite	-	-1.50	-6.92	0.70678	-	-	-	-	-	-	-	-
F1173	2.6	2.6	dgy lime micrite	-	-0.94	-8.53	0.70681	-	-	-	-	-	-	-	-
F1173	3.1	3.1	dgy lime micrite	-	-0.66	-8.41	0.70672	-	-	2763	176	0.062	98.0	-	0.01235



F1173	3.0	3.0	dgy lime micrite	-	-0.89	-8.73	-	-	-	-	-	-	-	-	-
F1173	3.7	3.7	dgy lime micrite	-	-	-	0.70675	-	-	-	-	-	-	-	-
F1173	4.3	4.3	dgy lime micrite	-	-0.74	-8.77	-	-	-	-	-	-	-	-	-
F1173	4.9	4.9	dgy lime micrite	-	-0.65	-8.80	0.70682	-	-	-	-	-	-	-	-
F1173	5.5	5.5	dgy lime micrite	-	-0.50	-8.78	0.70681	-	-	-	-	-	-	-	-
F1173	6.0	6.0	dgy lime micrite	-	-0.78	-9.03	0.70680	-	-	2825	439	0.149	96.0	-	0.03005
F1173	6.5	6.5	dgy lime micrite	-	-0.59	-8.83	-	-	-	-	-	-	-	-	-
F1173	7.0	7.0	dgy lime micrite	-	-0.67	-8.90	-	-	-	-	-	-	-	-	-
F1173	7.5	7.5	dgy lime micrite	-	-0.92	-8.60	0.70676	-	-	3345	209	0.061	98.0	-	0.01344
F1173	8.0	8.0	dgy lime micrite	-	-0.90	-9.25	0.70676	-	-	3052	210	0.069	100.0	-	0.01487
F1173	8.5	8.5	dgy lime micrite	-	-0.90	-9.03	-	-	-	-	-	-	-	-	-
F1173	9.0	9.0	dgy lime micrite	-	-0.93	-9.08	-	-	-	-	-	-	-	-	-
F1173	9.5	9.5	dgy lime micrite	-	-0.98	-9.07	0.70674	-	-	3808	137	0.035	98.0	-	0.01118
F1173	10.0	10.0	dgy lime micrite	-	-0.87	-9.26	-	-	-	-	-	-	-	-	-
F1173	10.5	10.5	dgy lime micrite	-	-0.51	-9.25	0.70682	-	-	2248	761	0.332	98.0	-	0.03263
F1173	11.0	11.0	dgy lime micrite	-	-0.34	-8.80	0.70685	-	-	2082	468	0.225	100.0	-	0.02748
F1173	11.5	11.5	dgy lime micrite	-	-0.25	-8.82	0.70677	-	-	3007	597	0.198	100.0	-	0.03911
F1173	12.0	12.0	dgy lime micrite	-	-0.55	-8.81	0.70681	-	-	2761	579	0.210	100.0	-	0.11319
F1173	12.5	12.5	dgy lime micrite	-	-0.62	-8.31	-	-	-	-	-	-	-	-	-
F1173	13.0	13.0	dgy lime micrite	-	-0.57	-9.16	-	-	-	-	-	-	-	-	-
F1173	13.5	13.5	dgy lime micrite	-	-0.28	-8.81	-	-	-	-	-	-	-	-	-
F1173	14.0	14.0	dgy lime micrite	-	-0.33	-7.93	0.70676	-	-	3512	1220	0.347	100.0	-	0.02686
F1173	14.5	14.5	dgy lime micrite	-	-0.16	-8.78	0.70679	-	-	2240	733	0.327	100.0	-	0.03638
F1173	15.0	15.0	dgy lime micrite	-	-0.26	-8.46	-	-	-	-	-	-	-	-	-
F1173	15.5	15.5	dgy lime micrite	-	-0.18	-9.03	-	-	-	-	-	-	-	-	-
F1173	16.0	16.0	dgy lime micrite	-	-0.77	-9.00	-	-	-	-	-	-	-	-	-
F1173	16.5	16.5	dgy lime micrite	-	-0.22	-9.21	0.70681	-	-	3084	663	0.206	95.9	-	0.03936
F1173	17.0	17.0	dgy lime micrite	-	-0.36	-8.50	0.70692	-	-	2924	905	0.297	96.0	-	0.10666
F1173	17.5	17.5	dgy lime micrite	-	-0.24	-6.51	0.70677	-	-	3340	1319	0.387	98.0	-	0.02427
F1173	18.0	18.0	dgy lime micrite	-	-0.38	-7.56	-	-	-	-	-	-	-	-	-
F1173	18.5	18.5	dgy lime micrite	-	-0.20	-9.15	-	-	-	-	-	-	-	-	-
F1173	19.0	19.0	dgy lime micrite	-	0.04	-9.02	0.70679	-	-	2372	509	0.202	94.1	-	0.03203
F1173	19.5	19.5	dgy lime micrite	-	0.04	-9.25	0.70683	-	-	2594	615	0.223	94.1	-	0.03571

F1173	20.0	20.0	dgy lime micrite	-	-0.09	-8.53	-	-	-	-	-	-	-	-	-
F1173	20.5	20.5	dgy lime micrite	-	-0.11	-9.23	0.70684	-	-	3240	662	0.200	98.0	-	0.02726
F1173	21.0	21.0	dgy lime micrite	-	-0.15	-9.81	0.70692	-	-	2062	538	0.250	96.0	-	0.02899
F1173	21.5	21.5	dgy lime micrite	-	-0.24	-8.66	-	-	-	-	-	-	-	-	-
F1173	22.0	22.0	dgy lime micrite	-	-0.03	-8.92	0.70686	-	-	2671	735	0.243	88.2	-	0.06239
F1173	22.5	22.5	dgy lime micrite	-	0.01	-9.01	-	-	-	-	-	-	-	-	-
F1173	23.0	23.0	dgy lime micrite	-	-0.60	-9.10	0.70681	-	-	3470	593	0.161	94.1	-	0.05661
F1173	23.5	23.5	dgy lime micrite	-	-1.50	-10.48	-	-	-	-	-	-	-	-	-
F1173	24.5	24.5	dgy lime micrite	-	-0.01	-8.79	-	-	-	-	-	-	-	-	-
F1173	25.0	25.0	dgy lime micrite	-	0.25	-8.62	-	-	-	-	-	-	-	-	-
F1173	25.5	25.5	dgy lime micrite	-	0.38	-9.14	0.70683	-	-	2675	381	0.140	98.0	-	0.03017
F1173	26.0	26.0	dgy lime micrite	-	0.34	-9.20	-	-	-	-	-	-	-	-	-
F1173	26.5	26.5	dgy lime micrite	-	0.09	-9.17	-	-	-	-	-	-	-	-	-
F1173	27.0	27.0	dgy lime micrite	-	0.73	-5.28	0.70684	-	-	1513	703	0.446	96.1	-	0.09318
F1173	27.5	27.5	dgy lime micrite	-	-0.68	-8.46	0.70687	-	-	2898	455	0.154	98.0	-	0.11465
F1173	28.0	28.0	dgy lime micrite	-	-0.23	-8.73	0.70701	-	-	2283	483	0.181	85.7	-	0.14863
F1173	28.5	28.5	dgy lime micrite	-	0.29	-7.65	-	-	-	-	-	-	-	-	-
F1173	29.5	29.5	dgy lime micrite	-	-0.02	-9.85	0.70692	-	-	2454	300	0.103	84.0	-	0.04424
F1173	30.0	30.0	dgy lime micrite	-	0.67	-9.90	-	-	-	-	-	-	-	-	-

(d)gy = (dark)grey, gs = grainstone, wacke = wackestone, ev = evaporite, wht = white, brecc = brecciated, dol = dolomite

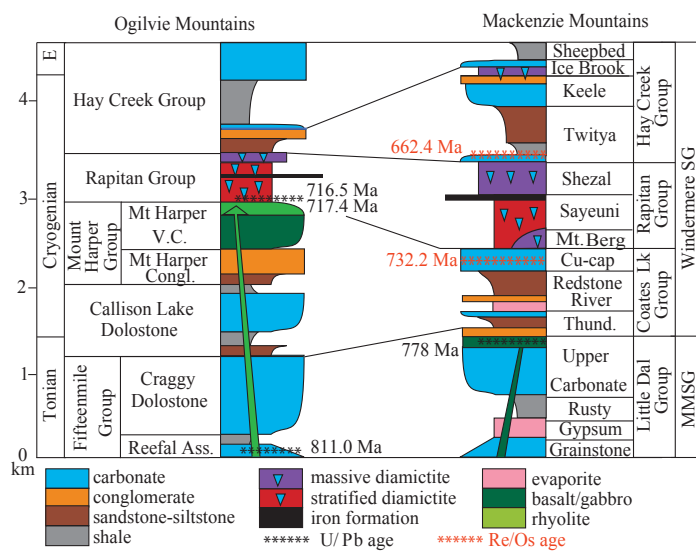


Figure 1

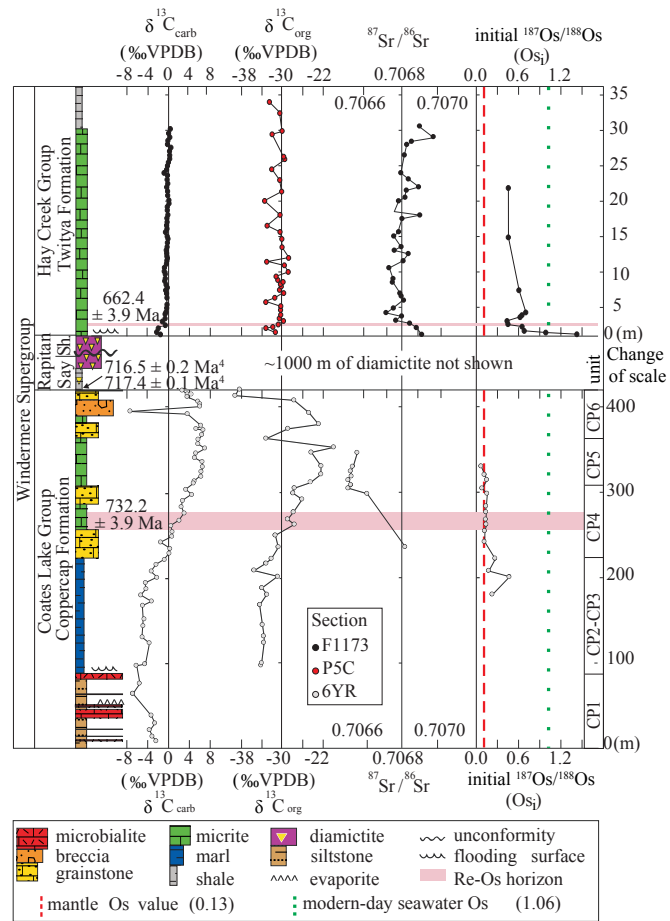


Figure 2

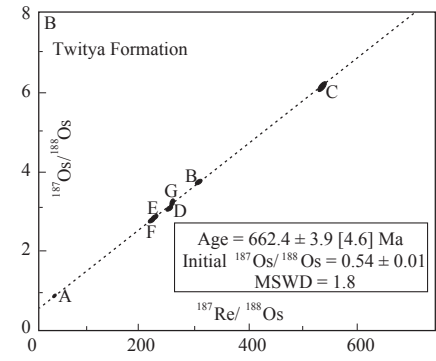
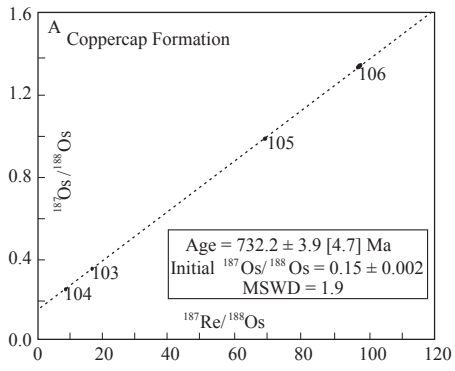


Figure 3

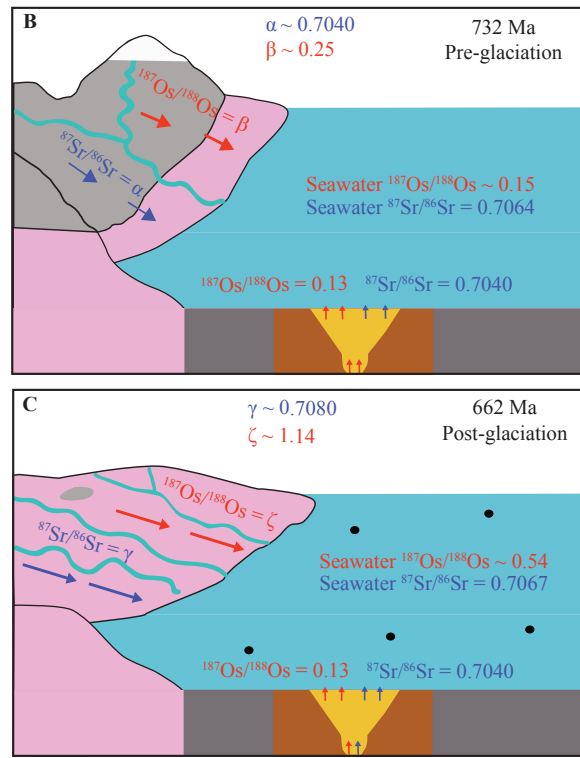
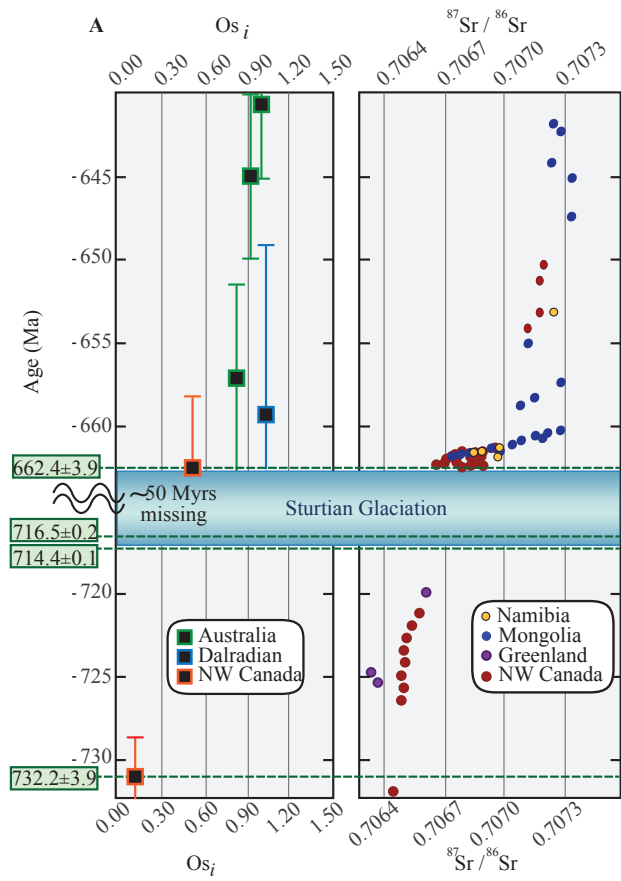


Figure 4

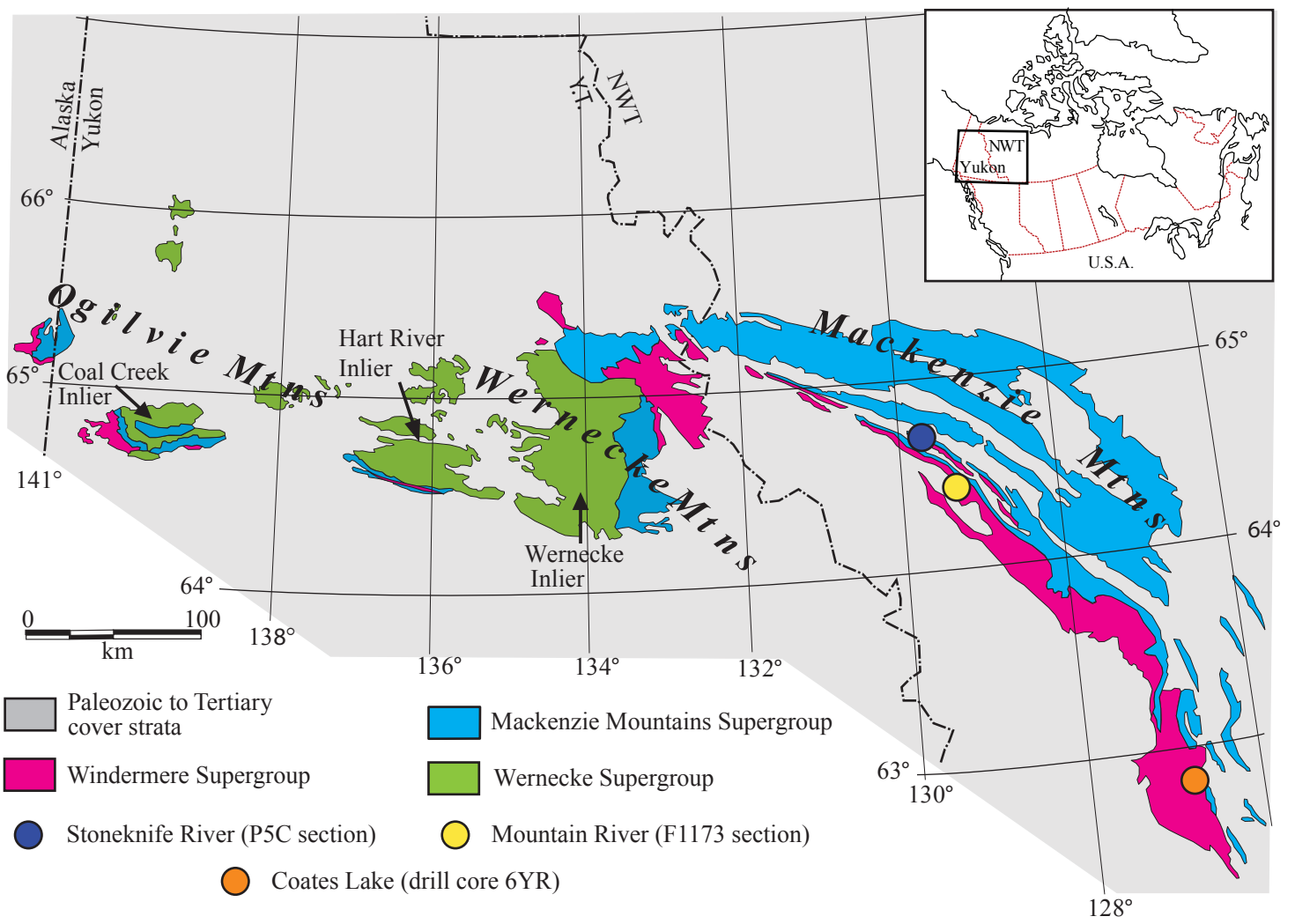


Figure S1

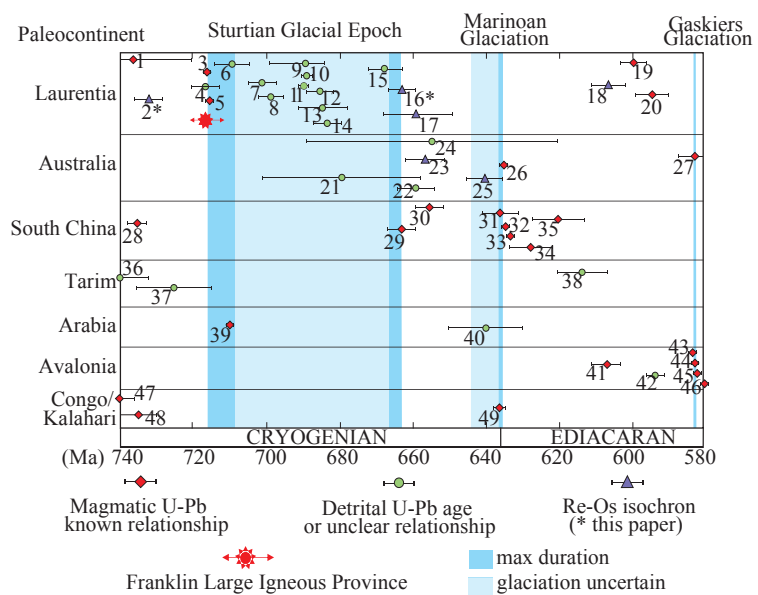


Figure S2